Journal of Power Sources 196 (2011) 13–24

Contents lists available at ScienceDirect

Journal of Power Sources

journal homepage: www.elsevier.com/locate/jpowsour

Review

A review of the electrochemical performance of alloy anodes for lithium-ion batteries

Wei-Jun Zhang

Department of Mechanical Engineering, Virginia Commonwealth University, 401 West Main Street, Richmond, VA 23284, United States

ARTICLE INFO

Article history:
Received 7 July 2010
Accepted 7 July 2010
Available online 13 July 2010

Keywords:
Lithium-ion batteries
Alloy anodes
Energy density
Cycle life
Capacity loss

ABSTRACT

Alloy anodes are promising anode materials for lithium-ion batteries due to their high-energy capacity and safety characteristics. However, the commercial use of alloy anodes has been hindered to date by their low cycle life and high initial capacity loss. This review highlights the recent progress in improving and understanding the electrochemical performance of various alloy anodes. The approaches used for performance improvement are summarized, and the causes of first-cycle irreversible capacity loss are discussed. The capacity retentions and irreversible capacity losses of various alloy anodes are compared. Several alloy anodes exhibited excellent cycle life (up to 300 cycles) with high initial coulombic efficiency (80–90%) and large reversible capacity (500–700 mAh g^{-1}).

Contents

1. Introduction

Lithium-ion batteries are the primary energy storage devices in the communications, transportation and renewable-energy sectors [1,2]. The current choice of anode materials for lithium-ion batteries is graphite due to its long cycle life, abundant material supply and relatively low cost. However, the graphite anode has the disadvantages of low energy density (375 mAh g^{-1}) and safety issues related to lithium deposition [3,4]. Thus, there has been a growing interest in developing alternative anode materials with low cost, enhanced safety, high-energy density and long cycle life [5].

Alloy anodes are known for their high specific capacity and safety characteristics [4–7]. Table 1 compares the electrochemical properties of alloy anodes, lithium metal, graphite and a new anode material, $Li_4Ti_5O_{12}$ (LTO). The theoretical specific capacities

E-mail address: zweijun@vcu.edu.

0378-7753/$ – see front matter © 2010 Elsevier B.V. All rights reserved.
doi:10.1016/j.jpowsour.2010.07.020

Table 1
Comparison of the theoretical specific capacity, charge density, volume change and onset potential of various anode materials.

Materials	Li	C	$Li_4Ti_5O_{12}$	Si	Sn	Sb	Al	Mg	Bi
Density ($g\,cm^{-3}$)	0.53	2.25	3.5	2.33	7.29	6.7	2.7	1.3	9.78
Lithiated phase	Li	LiC_6	$Li_7Ti_5O_{12}$	$Li_{4.4}Si$	$Li_{4.4}Sn$	Li_3Sb	LiAl	Li_3Mg	Li_3Bi
Theoretical specific capacity ($mAh\,g^{-1}$)	3862	372	175	4200	994	660	993	3350	385
Theoretical charge density ($mAh\,cm^{-3}$)	2047	837	613	9786	7246	4422	2681	4355	3765
Volume change (%)	100	12	1	320	260	200	96	100	215
Potential vs. Li (~V)	0	0.05	1.6	0.4	0.6	0.9	0.3	0.1	0.8

of alloy anodes are 2–10 times higher than that of graphite, and 4–20 times higher than that of LTO. Note that the charge densities (volumetric capacities) given in Table 1 were calculated using the density of pristine metal. Even if the full volume expansion of lithiated products is considered, the charge densities of alloy anodes are still 2–5 times higher than those of graphite and LTO. The second merit of alloy anodes is their moderate operation potential versus lithium. For example, both Si and Al anodes have an onset voltage potential of 0.3–0.4 V above Li/Li^+. This moderate potential averts the safety concern of lithium deposition as with graphite anodes (~0.05 V vs. Li), meanwhile, avoids the energy penalty of battery cells assembled with the LTO anodes (1.5 V vs. Li/Li^+).

The main challenge for the implementation of alloy anodes is their large volume change (up to 300%) during lithium insertion and extraction (see Table 1), which often leads to pulverization of the active alloy particles and poor cycle stability [7–9]. In addition, the first-cycle irreversible capacity loss of alloy anodes is too high for practical application. Extensive research has been carried out to address these two issues and significant progress has been made during the last two decades [10–198]. Progress on these issues has been periodically reviewed in several excellent articles in the areas of intermetallics [6,8], silicon-based or tin-based anodes [5,7,9] and battery materials [2,4]. The objective of the current review is to highlight the recent advance in fundamental understanding and engineering development of alloy anode systems. This report focuses on the electrochemical performance of alloy anodes including first-cycle irreversible capacity loss, cycle life, rate capacity and anode-design methodology. A future work will concentrate on the fundamental understanding of the lithium reaction mechanism and phase transformation during cycling. To simplify the discussion, the term "alloy anodes" is used in this paper to refer generally to metals, metalloids and alloy-compound anodes.

Many metals are reactive towards lithium, e.g., Si, Sn, Sb, Al, Mg, Bi, In, Zn, Pb, Ag, Pt, Au, Cd, As, Ga and Ge [7]. However, only the first five elements have been widely investigated because they are cheap, abundant and environmentally friendly. In this work, the electrochemical performance of Si, Sn, Sb and their alloys is extensively reviewed because most of the literature has been generated on these three alloy groups. The alloy anodes can be pure metals, alloys or intermetallic compounds, either in crystalline or amorphous state. They can be in the form of fine powders or thin films. We begin with a brief review of the common causes of the poor performance of alloy anodes, discuss the technologies used to overcome these hurdles, and then summarize the electrochemical performance of Si, Sn, Sb anodes and their alloys.

2. Cause of irreversible capacity and cyclic capacity fade

Low irreversible capacity and long cycle life are two basic requirements for advanced anode materials. Unfortunately, early studies found that many alloy anodes had high initial irreversible capacities (the difference between charge and discharge capacity) and rapid capacity fade during cycling (loss of reversible capacity) [10–17]. Fig. 1 shows an example of the charge/discharge curves of Si alloy anodes [18]. Here, it is evident that the delithiation capacity (charge) is much lower than the lithiation (discharge) capacity

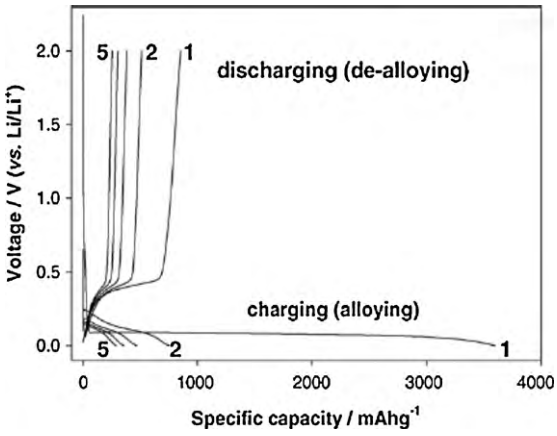

Fig. 1. Charge–discharge voltage profiles of a pure silicon anode with an average powder size of 10 μm. Reproduced from [18] with permission.

at the first cycle. The first-cycle irreversible capacity loss is high ($2650\,mAh\,g^{-1}$) and the coulombic efficiency is low (only 25%). Furthermore, the capacity decreased quickly during the following cycles; after five cycles the reversible capacity dropped by 70%. This type of behavior has been commonly observed in other alloy systems. The causes of large irreversible capacity for alloy anodes are considered to be the following:

(1) *Loss of active material*. Because of the large volume change during cycling, cracking and pulverization of active particles and the surrounding matrix lead to the disconnection of some alloy particles from the conductive carbon or current collector [11,13,16–21]. The cracking of alloy particles has been confirmed by SEM observation [22]. The breakdown of the conductive network between active particles and the carbon matrix was evidenced by the sharp rise of the internal resistance of a Si anode at ~0.4 V during the Li-extraction process [19,23]. Due to the large internal resistance and the isolation of Si particles, the delithiation reaction was not completed, with some Li remaining in the Si particles. As a result, an irreversible capacity loss was observed. Interestingly, Ryu et al. [23] observed that some of the lost capacity was recovered by applying pressure on the test cell as contact of the isolated particles with carbon was resumed.

The occurrence of severe Si particle breakdown at ~0.4 V during Li extraction is plausible because the particles are subjected to large tensile stresses in this process as a result of the large volume contraction. The initiation and propagation of microcracks is normally promoted by tensile stresses instead of compressive stresses unless the compressive stress is extremely high. Upon lithiation, both Si and the matrix are most likely under compressive stresses as a result of the volume expansion and thus the Si particles remain mostly intact. Upon delithiation, the contraction of Si particles results in large tensile stresses, leading to the cracking of Si particles or the surrounding matrix, especially when the volume contraction reaches the maximum at ~0.4 V. A detailed AFM study of the anode surface has also revealed

that cracking occurs mainly during the Li-extraction stage [21].

(2) *Formation of solid–electrolyte interface (SEI) films*. The formation of passivating SEI films on alloy particles was confirmed by HRTEM, FTIR and XPS as a result of lithium reaction with the electrolyte at the surface of alloy particles [15,22,24–26]. The SEI films consisted mainly of Li_2CO_3, various lithium alkylcarbonates ($ROCO_2Li$), LiF, Li_2O and nonconductive polymers. The composition of the SEI films formed on alloy anodes was different from that on graphite and it varied from alloy to alloy [15,22,26,27,189]. In graphite, a stable SEI film normally develops in the first cycle at 0.5–1.0 V versus lithium, and contributes mostly to the first-cycle irreversible capacity. In contrast, the SEI formation on alloy anodes appears to be a dynamic process of breaking off and reforming due to the constant volume changes of the alloy particles during cycling [17,26,27,192]. The thickness of SEI films and the amount of salt-degradation products have been observed to increase with the cycling number [22,26]. In addition, the freshly formed metal surface from particle cracking or displacement reaction (such as Co from CoSn) may act as a catalyst to promote SEI formation even at a relatively low voltage range (0.5–0 V) [26,28,29]. Metal particles were found to catalyze SEI formation on graphite anodes [199,200]. Therefore, the formation of SEI films on alloy anodes is expected to contribute to both the first-cycle irreversible capacity and the later cycle capacity fade.

(3) *Trapping in the host alloy*. Even though Li insertion/extraction in alloys is generally reversible, some Li ions may be permanently trapped in the alloys due to (a) slow Li release kinetics, (b) the formation of highly stable lithiated compounds or (c) strong bonding with less coordinated atoms at defect sites [11,13,30–35]. A high density of defects is expected at surface, interface or grain boundaries in alloy particles due to the large volume change and the complicated structural transformation in the Li-insertion/extraction process. Li can be trapped irreversibly at these defect sites [33,35,36]. Li insertion has also been reported to be incompletely reversible in Mg-containing alloys [11,37,38]. In addition, the presence of impurities such as S, P, O and C in host alloys may lead to the formation of stable lithium compounds, resulting in irreversible capacity loss [9].

(4) *Reaction with surface oxide layers*. Because many metals are reactive with oxygen or water, a passivation oxide layer is normally formed on a metal or alloy particle surface during material preparation. Li reacts irreversibly with many oxides to form Li_2O at the potential of approximately 0.8–1.6 V [15,26,39]. One extreme case is the tin-based amorphous oxide composites (CTOs), which are converted to nanocrystalline Sn and Li_2O during lithiation with a low coulombic efficiency of 63% [40,41]. Because of the low atomic weight of oxygen, even a small amount of oxide will lead to a large irreversible capacity loss. For example, the theoretical specific capacities of SnO_2 and SiO_2 are as high as 715 and 1784 mAh g^{-1}, respectively.

(5) *Aggregation of alloy particles*. Electrochemical aggregation has been observed in many fine-grained alloy anodes during cycling [15,33,35,41]. The reason for aggregation has been attributed to the welding effect induced by the pressure resulting from the large volume expansion [15]. The agglomeration of active particles results in the increase of Li diffusion length and the trapping of SEI films in the particles, leading to irreversible capacity loss [15].

3. Approaches for improving anode performance

In an attempt to reduce the cyclic capacity fade and the first-cycle irreversible capacity of alloy anodes, several strategies have been developed to reduce the detrimental effects of large volume changes and to alleviate the side reaction with electrolyte. These approaches are classified into the following six categories.

3.1. Multiphase composites

The primary purpose of dispersing active alloy particles within a composite matrix (filler) is to use the host matrix to buffer the large volume change of the active particles so that the electrode integrity and the electronic contact between the active particles and conductive phase can be maintained [42,171]. To this end, the host matrix must allow rapid transport of electrons and Li ions and maintain the microstructural stability of the whole anode [13]. The host matrix also acts as a spacer to reduce the aggregation of active particles during cycling [13,41]. Based on the type of host phase, composite anodes can be described as (a) inactive matrix, (b) active matrix, (c) carbon-matrix composite and (d) porous structures.

(1) *Inactive-matrix composites*. This type of composite anode consists of active particles and an electrochemically inert matrix [43,197]. The matrix can be a metal such as Fe, Cu or Nb [44,45,170], an alloy like $FeSi_2$ [46], an oxide such as Al_2O_3 [47,48,196] and Li_2O [49], or a ceramic such as TiN [50], SiC [51] and TiB [52]. A good example of this type is the tin-based composite oxide anode (CTO) formed by the in situ reaction of SnO with Li to create finely dispersed Sn nanocrystals in a mixed oxide matrix [40,53]. Composite anodes have shown excellent cycling stability for over 100 cycles at a reversible capacity of 600 mAh g^{-1} [40]. It has been widely reported that higher amounts of host phases improve the cycling stability of the anode but reduce specific capacity [13]. The buffering effect of the matrix was confirmed by SEM examination of a cycled Al anode, which showed that no cracking developed in an Al/SiC composite, whereas severe cracking was observed in the pure Al anode at the first cycle [51].

One potential drawback of the inactive host phases is that they may block or slow down lithium diffusion or electron transfer, resulting in a less-than-expected capacity [54]. To avoid this problem, the host matrix must possess good ionic and electronic conductivities and appropriate mechanical strength. In terms of mechanical properties, it has been proposed that a matrix with a high yield strength, low ductility and a low elastic modulus will provide better volume compensation during cycling [19,56]. In other words, the matrix must be able to sustain a high stress with a large elastic deformation when the active particles expand so that the active particles are under high compressive residual stress during Li insertion. A compressive residual stress was reported to prevent particles from cracking [23,57]. As mentioned earlier, cracking develops mainly under large tensile stresses. A high residual compressive stress in the particles during expansion will reduce the tensile stress level during particle contraction. In contrast, the facile plastic deformation of a matrix may relieve the large compressive stress in the particle during expansion (lithiation) leading to high tensile stress during contraction (delithiation) unless the matrix or the particle is cracked. In this view, a matrix with high strength, low ductility and a low elastic modulus may reduce the tendency for active particle cracking. Further study is warranted on this hypothesis.

(2) *Active-matrix composites*. In active-matrix anodes, both the active phase and the host matrix are reactive towards lithiation. The idea of an active composite is to have one component lithiated while the other acts as a buffer to alleviate the volume change as they react with Li at different onset potentials. For example in the SnSb alloy, the more active phase, Sb, begins Li insertion at ~0.9 V vs. Li/Li^+ while the second unre-

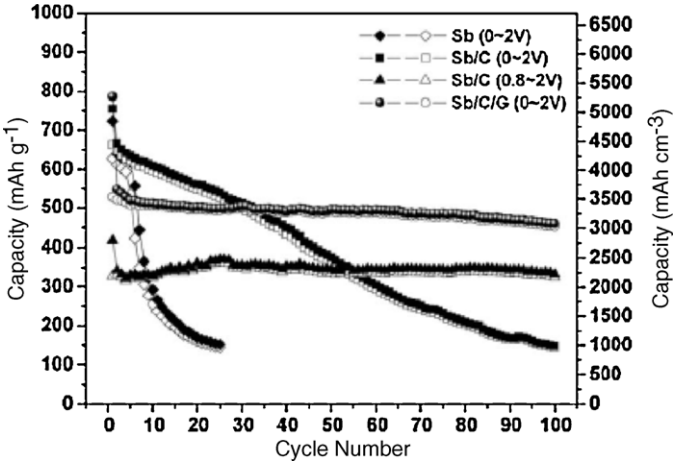

Fig. 2. Comparison of cycle performance for Sb, Sb/carbon and Sb/carbon/graphite nanocomposites under different voltage windows. Reproduced from [83] with permission.

acted component, Sn, with an onset potential of ~0.6 V, can thus accommodate the volume expansion of the lithiated Sb phase [14]. Among the active composites, the most studied alloys are SbSn [14–17,33,42,58–62,190], SbIn [6,63–68], $SbAg_3$ [16,20], SbAl [26,63], SnAg [69–71] and Mg_2Si [11,153]. The challenge for some of the active composite anodes is their low reversibility during repeated cycling. As a result, the cycle life of pure active-matrix anodes is often lower than that of the mixed active/inactive composites. In addition, it has been found that the cycling stability of active-matrix composites depends strongly on the charge depth. A better cycle life was achieved by controlling the charge to a limited state of second-component lithiation [13,61].

(3) *Carbon-based composites*. The beneficial effect of carbon addition or a carbon coating has been widely observed in many studies [47,57,62,74–80]. Carbon-matrix composites can be prepared by ball milling of active materials with graphite [69,81,82] or carbon black [37,62,77,83], or by pyrolysis of carbon precursors [49,57,74,75]. The improved cycling performance of carbon-matrix composites was attributed to the improved electric conductivity and the buffering effect of carbon [37,47,48,74,80]. Carbon additives also have the advantages of good ionic conductivity, low volume expansion, tolerance to mechanical stress and Li-storage ability [37,48,57]. In addition, the presence of a carbon coating on Si particles was believed to suppress the formation of SEI layers [57,78]. It has also been suggested that a carbon coating exerted a compressive stress on the active particles which acted as an opposing force against particle volume expansion during lithiation and thus limited the pulverization of the particles [57]. The compressive residual stress was considered to be important in enhancing the cycling performance of Si/C composite anodes because the performance deteriorated when the stress was relieved by grinding or annealing [57]. In general, higher carbon content leads to better capacity retention but at the expense of reducing the specific capacity and increasing the irreversible capacity loss [57,76,79,84].

The first-cycle irreversible capacity of carbon-composite anodes depends strongly on the carbon type and the preparation method, as further discussed in Section 4. Along with particle size control, several carbon nanocomposites exhibited stable cycle lives of over 100 cycles [47,62,83]. An example is given in Fig. 2, which shows that the addition of carbon (C) and graphite (G) improved the cycle life of a nanocrystalline Sb anode [83].

(4) *Porous structures*. One way to overcome the problem of large volume expansion is to design three-dimensional porous electrode structures with sufficient porosity to accommodate the volume expansion. A similar approach was employed in the high-temperature commercial $Na/NaCl_2$ cell [85]. Porous anode structures can be prepared by electrodepositing active materials such as Sn or Si onto a porous current collector [85–87] or onto a template [88,89]. The cycle performance of anodes deposited on a porous substrate was significantly improved compared to those deposited on a planar collector [86,90,91]. For example, a silicon anode deposited on a Ni foam current collector showed a stable cycle life of over 400 cycles at a reversible capacity of ~500 mAh g^{-1} [86]. However, the presence of a large volume of pores in the porous electrodes decreases the total volumetric energy density of the cell. Therefore, the challenge for porous-structure electrodes is to increase the active material loading to a practically acceptable level [89].

3.2. Particle size control

It has been confirmed in many studies that reducing the active particle size to the nanometer range (<100 nm) can significantly improve the cycling performance of alloy anodes, especially when agglomeration of the particles is inhibited by a composite matrix [13–15,39,42,50,52,75,84,92–96,172]. Early studies by Yang et al. [13,42] found that when the particle size of Sn powders was decreased from 3 μm to 300 nm, the number of stable cycles increased from 3 to 70. In a recent paper, a nanosized SnSb/C composite prepared by high-energy ball milling exhibited a cycle life of more than 300 cycles [62]. A nanocrystalline $Sb/Al_2O_3/C$ composite also showed excellent cyclic stability of over 100 cycles [47].

The improved cycling stability was attributed primarily to the ability of nanosized particles to accommodate large stress and strain without cracking [42,93]. It is well known that as the grain size is decreased to nanometer scale, the yield and fracture strengths of metals and alloys increase dramatically (by several fold) because the motion and pile-ups of dislocations (responsible for the early cracking and fracture) are constrained or eliminated in nanosized grains or particles [201,202]. This implies that nanocomposite anodes can sustain much higher stresses before pulverization. In fact, cracking has rarely been observed in nanosized alloy anodes. In addition, a smaller particle size decreases the electronic and ionic transport distance and reduces the stress or strain induced by inhomogeneous Li diffusion [52,96]. The high density of grain boundaries in nanocomposites also provides a fast diffusion path for Li ions and act as additional Li-storage sites [95]. Lithium insertion at grain boundaries may also reduce the total volume expansion of anodes because the packing density at nanocrystalline boundaries is somewhat lower than that of the perfect crystal by 10–30% [72,203].

However, it is worth keeping in mind that nanosized particles have many disadvantages such as large surface area, high manufacturing cost and handling difficulty [2,39]. The existence of large surface areas increases the side-reactions and SEI formation, which may lead to self-discharge, poor cycling life and short calendar life. One possible way to overcome these problems is to prepare anode composites comprised of large primary particles and nano-grained secondary particles. This approach has been employed in several studies [5,47,62,83].

3.3. Intermetallics

The concept of intermetallic anodes was introduced and extensively investigated by Thackeray et al. [6,8,64,67,97,173]. The idea is to create a Li-insertion host structure that maintains a strong

structural relationship between the parent, intermediate and lithiated phases with a limited volume expansion during reaction [6,8,97,98]. This type of anode works similarly to the commercial high-temperature Zebra cell in which Ni in $NiCl_2$ is replaced by Na during reaction [6]. An important feature of intermetallic anodes is the existence of a stable sublattice corresponding to the graphite layers in carbon, but this sublattice is not widely spaced for Li intercalation [67]. Instead, Li insertion in the host lattice takes place by the concomitant extrusion of the second component. For example, in a Cu_2Sb anode Li inserts into the Cu_2Sb structure to form Li_2CuSb by concomitant extrusion of Cu and it finally yields Li_3Sb without disrupting the fcc Sb host sublattice [99]. The intermetallic anodes currently being extensively studied include Cu_6Sn_5 [44,85,100,101], InSb [64,67,68], Cu_2Sb [34,66,98,99,102,103] and CoMnSb [103,104]. Several intermetallic anodes have shown stable cycling performance for over 25 cycles [6,85,99,100]. The good cycling stability was attributed to the structural similarity, the limited volume change and the fast reaction kinetics provided by the reversible lithium insertion/metal extrusion. However, the specific capacities of these intermetallic anodes were relatively low (250–400 mAh g^{-1}) [99,100,104]. It would be highly desirable to develop novel intermetallic anodes with high specific capacity.

Another concept similar to intermetallics is the use of solid-solution alloy systems such as Mg–Li binary alloys, in which Mg forms a solid solution with Li over a wide composition range (from 30 at.% to nearly 100 at.% Li) [5,37,174]. As expected, a structural similarity can be maintained during this entire Li alloying range. However, the challenges for Mg–Li alloy implementation are the potential safety concerns due to the very low potential of Mg versus Li and the difficulty of preparing homogeneous Mg-alloy materials because of its high reactivity [5,174].

3.4. Thin film and amorphous alloys

The excellent cycling performance of thin-film Si anodes has been reported by a number of studies, with stable capacity retentions of over 2000 mAh g^{-1} for up to 1000 cycles [105–108]. The good capacity retention of thin-film anodes was attributed to the strong adhesion of active material to the conductive support. Thin-film anodes can be prepared by magnetron sputtering [111–113] or physical vapor deposition [108–110]. The performance of thin-film anodes depends strongly on the deposition rate, deposition temperature, substrate-surface roughness, film thickness and post-annealing treatment [107,115,114]. Most of the thin-film anodes prepared to date have been in an amorphous state. Takamura et al. reported that an amorphous Si thin film deposited 50 nm thick on a Ni foil exhibited a high specific capacity of over 2000 mAh g^{-1} and superior cyclability of over 1000 cycles at a charge rate of 12C [105,108]. However, the cycle life was dramatically reduced when the film thickness was increased (200 cycles for 0.5–1 μm films and 50 cycles for 1.8-μm films) [115]. The poor performance of thicker films (>1 μm) compared to thinner films was due to the increased Li diffusion length, higher electrical resistance and larger internal stress of Li insertion/extraction [86,117]. The challenges for thin-film anodes are (a) the high cost of the deposition process and (b) low active material loading [86,118].

In addition to pure Si films, various binary or ternary thin-film anodes were investigated by Dahn et al. [113,119–123,175] and others [117,124–126,193]. The alloys under study include Sn–Ni [126], Sn–Zr [124,125], Si–M (M = Mg, Al, Sn, Zn, Ag, Fe, Ni, Mn) [113,117,123,193] and Si–Al–M alloys [120,121,127]. Dahn et al. found that the composition of the films had a large impact on its cycling performance and amorphous films generally had better capacity retention and lower irreversible capacity than crystalline ones [113,120,122]. The advantage of amorphous materials was claimed to originate from the elimination of two-phase structures with different lithium concentrations, leading to more homogeneous volume expansion and improved charge–discharge cycling behavior [119].

3.5. Operating voltage control

It has been observed in many studies that alloy anodes have much better cycle life when they are cycled within a limited voltage range as compared to the full voltage range [14,20,65,80,83,92,128–130,168]. Cycling stability can be improved by restricting either the upper or lower cutoff voltage, which reduces the amount of volume change, the tendency for particle aggregation and the extent of structural change [20,92,132,133]. For example, limiting the reaction voltage of InSb and Ag_3Sb to the lithium-insertion/metal-extrusion stage (to >0.65 V for InSb and >0.2 V for Ag_3Sb) significantly improved the reversible reaction [20,64,65]. In contrast, if the extruded metals, such as Ag or In, were allowed to react fully with lithium to yield Li_4Sn and Li_4Ag in a full voltage cycle, the capacity of the cells declined rapidly. Fig. 2 shows that raising the low cutoff potential from 0 V to 0.8 V remarkably improved the cycling performance of an Sb/C nanocomposite [83]. Similarly, changing the lower cutoff voltage from 0 V to 0.2 V increased the cycle life of an amorphous Si anode from 20 to 400 cycles [168]. It has been suggested that the lithiated amorphous Si is suddenly converted into crystalline $Li_{15}Si_4$ below 50 mV, resulting in high internal stress and capacity fade [132,133]. Reducing the upper voltage of a nano-Si anode from 2 V to 0.8 V also led to improved capacity retention [80]. However, the shortcoming of voltage control is that it reduces anode capacity. For example, the specific capacity of an amorphous Si anode decreased from over ~3000 to ~400 mAh g^{-1} when the lower potential was increased from 0 V to 0.2 V [168].

3.6. Binder and electrolyte

In the preparation of a battery cell the active anode particles are mixed with conductive carbon particles and a binder (5–15 wt.%). The conventional binder used for graphite and alloy anodes is polyvinylidene fluoride (PVDF), a thermoplastic material with poor elastomeric properties. It is thus reasonable to expect that an alternative elastomer binder may have a better ability to accommodate the large volume change of alloy particles than PVDF [118,134]. This idea was proven effective for improving the cycling stability of different alloy anodes using cross-linking polymers and an elastomer binder system [118,135,136]. However, the concept was challenged by the finding that a stiff, brittle sodium carboxymethyl cellulose (CMC) binder was even more effective in enhancing the capacity retention of Si anode than either PVDF or the SBR elastomer binder [84,137,195]. This finding suggests that other factors also play an important role in addition to elastic elongation.

Li et al. [137] proposed that the CMC binder may act as a surface modifier promoting the formation of a stable SEI passive layer. Lestriez et al. [179] believed that the extended confirmation of CMC in solution led to a more homogeneous dispersion and networking of the conductive carbon and active particles. Winter et al. [180] reported that the formation of a strong chemical bond between the binder and the active particles (Si) was the major reason for the improved reversibility of an Si/C electrode prepared with a CMC binder. They suggested that the cohesive strength between the binder and active particles is an important factor. This hypothesis was supported by a previous report that replacing the PVDF binder with a modified acrylic adhesive increased the capacity retention of a Si/C electrode from 67% to 90% (50 cycles). The peel strength of the acrylic adhesive (7 N) was much higher than that of PVDF (0.4 N) [181]. By the same token, the use of a high-strength

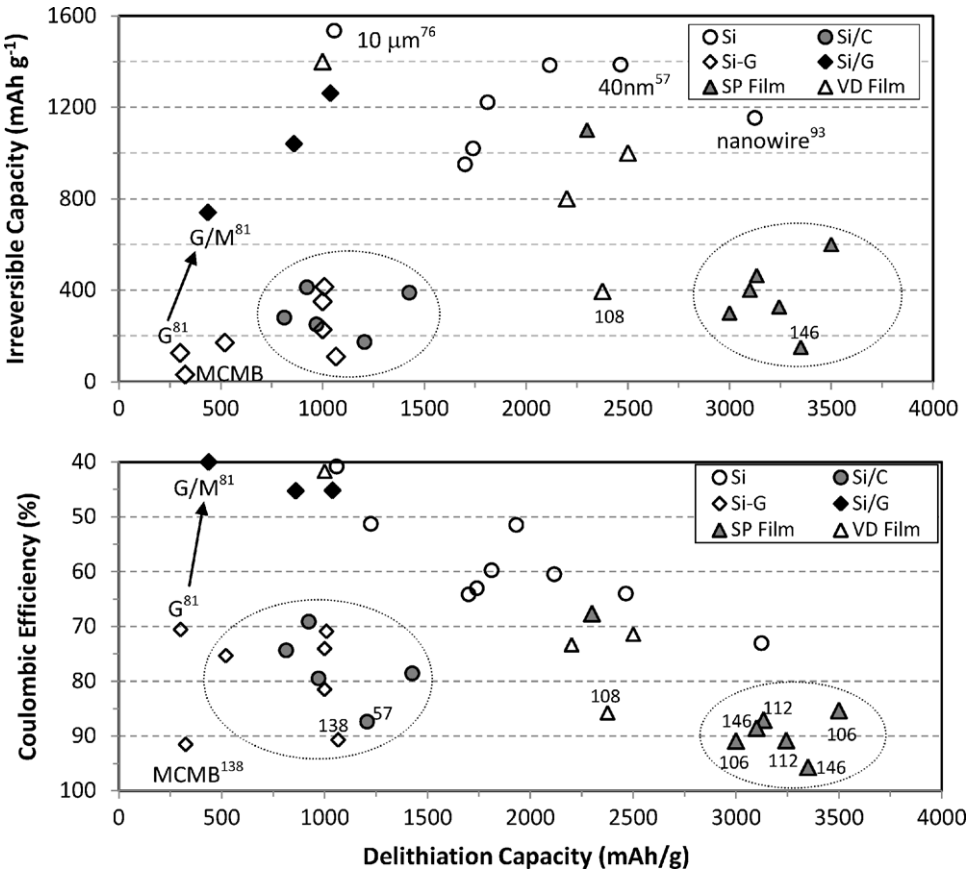

Fig. 3. The first-cycle irreversible capacity loss (a) and coulombic efficiency (b) of pure Si (Si) [23,57,76,80,93,94,138,139], Si with in situ formed carbon (Si/C) [57,75,141], Si with mildly mixed graphite (Si–G) [138,142–145], Si with extensively milled graphite (Si/G) [81,82], Si thin films prepared by magnetron sputtering (SP film) [106,111,112,114,146] and Si-thin-film anodes prepared by vacuum deposition (VD film) [108–110]. The numbers marked in the graph are reference numbers.

polyamide-imide (PAI) binder instead of PVDF increased the initial coulombic efficiency of a Si-based electrode from 29% to 75% [182]. In a recent paper, Dahn et al. [183] reported that a lithium polyacrylate (Li-PAA) binder performed even better than the CMC binder. An amorphous SnCoC electrode using a Li-PAA binder showed an excellent capacity retention of 450 mAh g^{-1} for at least 100 cycles as compared to less than 20 cycles when using the PVDF or CMC binders. These results indicated that the choice of binder system has a critical impact on the performance of alloy anodes. More studies are needed to understand the promoting effects of different binder systems.

In addition to the binder, the electrolyte composition also has an important effect on the cycle stability of alloy anodes [17,84,118,184–187,192]. Wachtler et al. [17] first reported that the reaction of electrolyte with the anode can be retarded by the use of a film-forming agent and surfactant additives. Subsequently, it was found that the concentration of ethylene carbonate or LiBOB in the electrolyte affected the cyclic capacity retention of alloy anodes [184,185]. The addition of succinic anhydride or fluoroethylene carbonate (FEC) to the electrolyte solution has been reported to greatly enhance the cycling performance of alloy anodes [186,187]. The addition of 3% FEC in an ethylene carbonate/diethyl carbonate/$LiPF_6$ electrolyte increased the capacity retention of an amorphous Si thin-film electrode from 68% to 88% after 80 cycles [187]. The improvement was attributed to the formation of a dense SEI layer consisting of stable compounds. Along with binder selection, selecting an appropriate electrolyte appears to be critical for the successful commercialization of alloy anodes.

4. Electrochemical performance of various alloy anodes

By employing the various approaches discussed in Section 3, the electrochemical performance of alloy anodes has been significantly improved. In this section, the first-cycle irreversible capacity, cycle life and rate capacity of three most studied systems (Si, Sn and Sb) are summarized.

4.1. First-cycle irreversible capacity

Silicon has been extensively investigated as an anode material because of its high theoretical energy capacity (Table 1). Fig. 3 summarizes the first-cycle irreversible capacity (IRC) and coulombic efficiency (COE) of various Si anodes. The pure Si powder anodes (Si) had a high IRC of 900–1100 mAh g^{-1} and a COE of 35–75% [23,57,76,80,93,94,138,139]. These pure Si powders were mostly in crystalline form before charging. However, after the first cycle, many of them converted into amorphous powders. Reducing the particle size from 10 μm to 10–40 nm slightly decreased the IRC and increased the COE because the nano-Si anodes [76,93,94] normally had a higher reversible capacity than the coarse Si samples [23,57,76]. However, even the nanowire Si anode (90 nm in diameter) [93] had a high IRC of 1150 mAh g^{-1} and a COE of 73%. The high IRCs of pure Si powders appear to be related to cracking-induced active material loss.

Generally speaking, adding carbon to Si powders significantly reduces the IRC, but the effect depends on the carbon type, carbon content and synthesis method [57,75,81,194]. The Si/C composites prepared by in situ pyrolysis of precursors such as polyvinyl chlo-

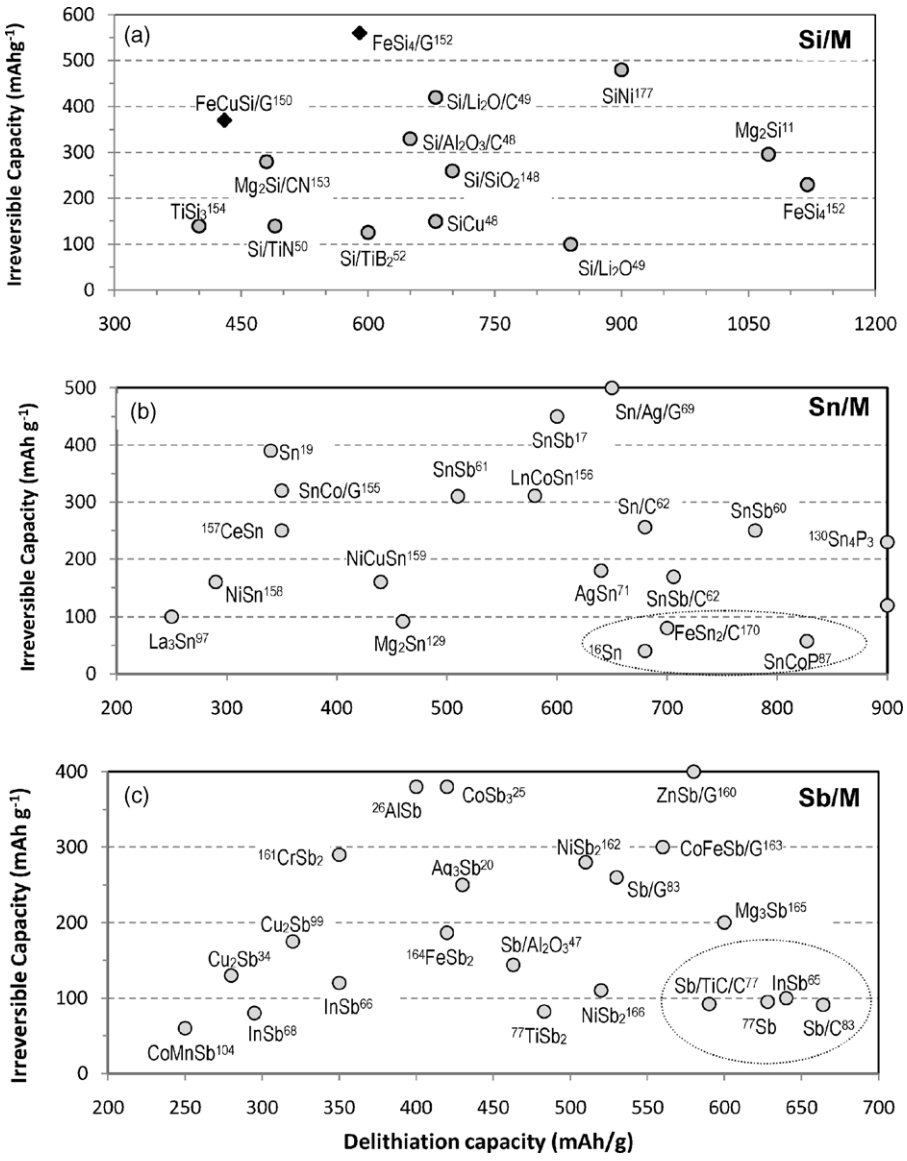

Fig. 4. The first-cycle irreversible capacity versus delithiation capacity of (a) Si-based, (b) Sn-based and (c) Sb-based alloy anodes. The reference numbers are given in the graphs as superscripts.

ride (Si/C) [57,75,141] or by mild mixing of Si particles with graphite (Si–G) [138,142–145] had low IRCs (200–400 mAh g^{-1}) and high COEs (70–90%). However, the Si/G composites prepared by extensive milling of Si with graphite had high IRCs (1000–1300 mAh g^{-1}) and low COEs (~45%) [81,82]. The low IRCs of both Si/C and Si–G powders appear to result from the buffering and coating effects of the dense carbon matrix [57,81,141]. The IRCs of the pure carbons prepared in situ from a polyvinyl chloride precursor were also low [117]. The high IRCs of milled Si/G composites originate from the high IRC of milled graphite. Milling of graphite was found to significantly increase its IRC (from 120 to 740 mAh g^{-1}) and decrease its COE (from 80 to 40%) as a result of the increased surface areas [81,149]. Therefore, it is very important to control the IRC of carbon in preparing carbon-matrix anode composites. Reducing Si particle size has no significant effect on IRC but improves capacity retention [75].

As shown in Fig. 3, the IRCs of Si-thin-film anodes (primarily amorphous films) also depend strongly on the preparation method. Most of the thin films prepared by magnetron sputtering (SP Film) had low IRCs (150–500 mAh g^{-1}) and high COEs (85–95%) [106,111,112,114,176], whereas the thin films prepared by vacuum deposition (VD Film) had relatively high IRC (800–1400 mAh g^{-1}) and low COE (40–75%), except for one sample [108–110]. The high IRCs of the VD films are likely due to the formation of SEI or stable Li compounds as a result of the high impurities in the films because the large irreversible capacity loss was observed at above the onset potential of Si lithiation (~0.4 V) in the first alloying cycle [109,110]. The IRC decreased with increasing film thickness or deposition rate [160,108,111]. When the Si target in vacuum deposition was heated to a high vaporization temperature, impurities such as O and H may easily react with the Si target or with the Si clusters leading to high impurity content. Thus, it is vitally important to carefully optimize the deposition conditions to reduce the IRCs of thin-film anodes. The observed high COEs of the SP Si films (>90%) are very encouraging. These indicate that low COE (high IRC) is not an intrinsic characteristic of alloy anodes. It is practicable to control the IRC of alloy anodes to a level comparable to that of the best carbon anodes (the MCMB carbon shown in Fig. 3) [4,138].

Fig. 4a compares the IRCs of Si alloy anodes and Si inactive-matrix composites (mostly in crystalline form). The IRCs of these samples are in the range of 100–500 mAh g^{-1}, comparable to the Si carbon-matrix composites (Fig. 3a). However, the reversible capaci-

ties of these anodes are relatively low except for the Si/LiO_2 sample [49]. As in Si/carbon composites, the high IRCs of several Si alloy anodes likely result from the high IRCs of the milled graphite or the porous carbon matrix in these samples [49,150,152].

Fig. 4b and c summarize the IRCs of various Sn-based and Sb-based alloy anodes. These alloys were mainly in crystalline form. The IRCs of these samples vary greatly from 40 to 600 mAh g^{-1}. Note first that all the samples with milled graphite additives had relatively high IRC values of 250–500 mAh g^{-1} [69,83,150,155,160,163]. Second, several Co-containing anodes also had high IRCs (300–400 mAh g^{-1}), including $CoSb_3$ [25], CoFeSb [163], LnCoSn [156], SnCo [155] but not the SnCoP sample, which was prepared by electroplating [87]. It is unclear whether the high IRCs of Co-containing alloys are due to oxide impurities or due to the catalytic effect of Co on SEI formation. The high IRCs (250–500 mAh g^{-1}) of nanosized Sn [19,62,69,156] and SnSb [17,60,61] anodes are at least partially due to the oxide impurities and SEI formation because a large capacity loss was observed at >0.7 V in first alloying cycle [17,19,61]. The high IRCs of AlSb [26] and $NiSb_2$ [162] were attributed to SEI formation. Compared to antimony, tin is more prone to oxidation; therefore, care must be taken to avoid it when preparing ultrafine Sn-based powders.

In Fig. 4, it is very encouraging to see that several Sn- and Sb-based anodes had a low IRC below 100 mAh g^{-1} and a high COE of 85–95% (marked by the dotted circles). Among these, the thin-film Sn anode prepared by electroplating (a few microns in thickness) had a high COE of 94% and a low IRC of ~40 mAh g^{-1} [16]. This result further demonstrates that the IRC of alloy anodes can be optimized to a level comparable to that of the best carbon anodes. In other words, high IRC is not an intrinsic character of alloy anodes. The crystalline SnCoP sample, with a high COE of 93% and a low IRC of ~60 mAh g^{-1}, was also prepared by electroplating [87]. The low IRCs of these two electroplated samples are likely related to their high purity and good electrical conductivity. The $FeSn_2/C$ [170] and InSb [65] samples, with COEs of 87–90%, were prepared by ball milling under argon. The Sb/C [83] and Sb/TiC/C [77] samples, with a COE of ~87%, were prepared by high-energy ball milling with Super P carbon black under argon. This result is surprising considering the high IRC (~500 mAh g^{-1}) and low COE (54%) of the milled-carbon black alone [62]. The low IRCs of these milled-carbon composites are probably because the composite powders consisted mainly of larger, micron-sized primary particles with the nanosized Sb particles embedded in the dense carbon matrix [62,83].

4.2. Capacity retention and cycle life

The capacity retention of alloy anodes has been substantially improved by the approaches outlined in Section 3. Fig. 5 shows the excellent cycling performance of three Sn-base alloys. The nanocrystalline $Sn_{30}(CoFe)_{30}C_{40}$ sample was an inactive-matrix carbon nanocomposite prepared by mechanical attrition [167]. This material showed a reversible capacity of ~430 mAh g^{-1} for at least 100 cycles and an IRC of ~85 mAh g^{-1}. The second sample, SnAg, was an active-matrix nanocomposite prepared by mechanical alloying [71]. This anode had a cycle life of over 300 cycles and a reversible capacity of ~330 mAh g^{-1} under a controlled cycling-voltage range (0–1.0 V). The SnSb/C nanocomposite was an active carbon-matrix composite prepared by high-energy ball milling. It had a microstructure consisting of nanosized SnSb (~10 nm) crystallites uniformly distributed in an amorphous carbon matrix [62]. The carbon content (Super P) in this composite was ~40 wt.%. This nanocomposite exhibited excellent cyclability for over 300 cycles at a stable capacity of ~560 mAh g^{-1}. The long cycle life of this nanocomposite was attributed to its small particle size and the buffering effect of the amorphous carbon matrix. No cracking was observed in the nanocomposite after extensive cycling, and the size

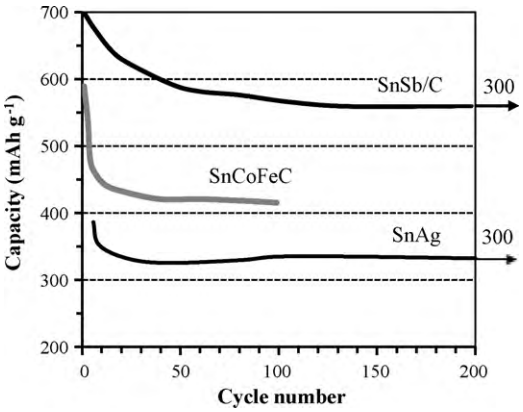

Fig. 5. The cycling performance of three tin-based alloy anodes: SnSb/C [62], SnAg [71] and $Sn_{30}(CoFe)_{30}C_{40}$ [167] alloys.

of the SnSb crystallites decreased to 2–3 nm at the tenth cycle. This material also exhibited good initial coulombic efficiency (~81%) and excellent high-rate capacity [62].

Fig. 6 shows the good cycling performance of Sb-based alloy anodes. The carbon-matrix nanocomposites Sb/C/G [83], Sb/TiC/C [77] and $Sb/Al_2O_3/C$ [47] were prepared by ball milling or mechanochemical milling, and their Sb contents by weight were 40%, 58% and 46%, respectively. Sb nanocrystallites of about 20 nm were uniformly dispersed through the carbon/ceramic matrix. All three nanocomposites had an excellent cycling life of over 100 cycles and a stable reversible capacity of 450–550 mAh g^{-1}. The Sb/TiC/C composite also had a high initial coulombic efficiency of 87% [77]. In addition, two intermetallic anodes, Cu_2Sb [99] and LiMgSb [165], showed stable cycling performance for over 20 cycles (test interrupted).

The excellent cycling performance of Si-base nanocomposites is presented in Fig. 7. Both the Si/40C (40 wt.% carbon) [149] and Si/80C (80 wt.% carbon) [142] nanocrystalline composites were prepared by in situ pyrolysis of carbon precursors. As a result, Si particles of 50–80 nm were homogeneously dispersed within the porous amorphous carbon matrix. These nanocomposites exhibited an excellent cycling stability of 100 cycles at the high reversible capacities of 1450 and 950 mAh g^{-1}, respectively. However, the first-cycle COEs were relatively low (~75%). The $Si/Li_2O/C$ nanocomposite [49] was prepared by mechanochemical reaction of SiO with lithium metal followed by in situ pyrolysis of a carbon precursor (PVC). The resulting porous nanocomposite (Si ~ 60 nm) had a stable cyclability of over 100 cycles and a capacity fade rate of ~0.15% per cycle, but its initial coulombic efficiency (COE) was only 60%. The Si/SiOx/C nanocomposite [148] was

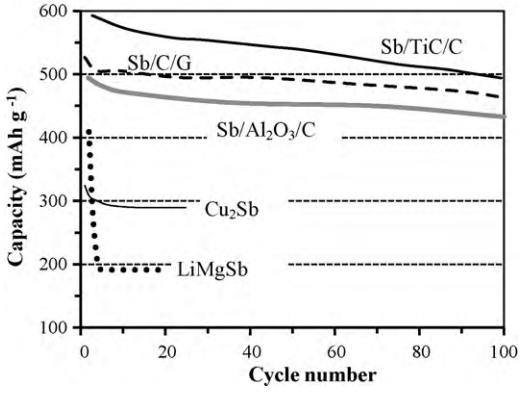

Fig. 6. The cycling performance of Sb-based alloy anodes: Sb/C/G [83], Sb/TiC/C [77] and $Sb/Al_2O_3/C$ [47] nanocomposites, Cu_2Sb [99] and LiMgSb [165] intermetallics.

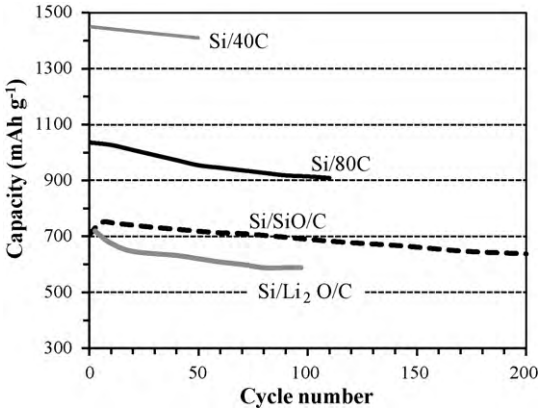

Fig. 7. The cycling performance of Si-based alloy anodes: Si/40C [149], Si/80C [142], Si/SiOx/C [148] and Si/Li_2O/C [49] nanocomposite anodes.

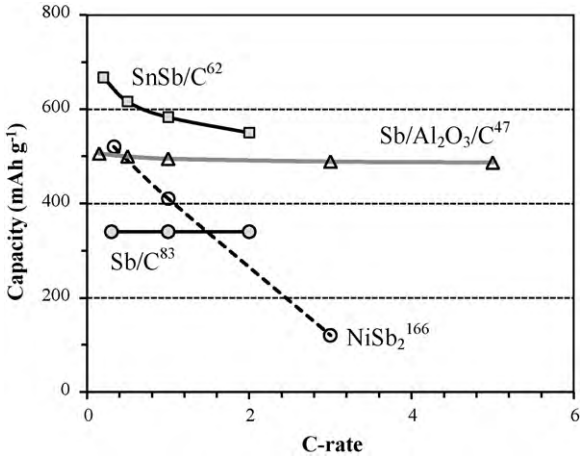

Fig. 8. The influence of C rate on the specific capacities of several alloy anodes. The reference numbers are given as superscripts.

synthesized by ball milling SiO and graphite powders followed by annealing at a high temperature with a carbon precursor. It had a microstructure consisting of Si nanoclusters (2–10 nm) dispersed in a silicon-oxide/carbon matrix. This material had a reversible capacity of ~700 mAh g^{-1} for up to 200 cycles and a capacity fade rate of 0.07% per cycle, but its COE was low (70%). These examples demonstrated that excellent cycling performance can be obtained with Si/C nanocomposite structures, but the initial irreversible capacity of these alloys needs further improvement.

In addition, several Si thin-film anodes (amorphous) exhibited long cycle life, up to 3000 cycles [106–108,110,112,168]. Takamura et al. reported a 50-nm Si thin film having a capacity retention of over 2000 mAh g^{-1} for 3000 cycles at a current rate of 30C [108], and a 670-nm film cycled for over 200 cycles at a similar capacity level [115]. A multilayer Fe/Si-film anode (138 nm) also showed a stable capacity of over 3000 mAh g^{-1} for 300 cycles [107]. As mentioned earlier, the challenge for thin-film anodes is to increase the film thickness to a level suitable for practical applications.

Finally, it is worth noting that the electrochemical performance of alloy anodes in many of the studies mentioned above was evaluated in a half-cell using lithium metal as a counter electrode. The conditions in a half-cell are different from a standard Li-ion cell because of the constant supply of lithium in the half-cell. In the case of continuous consumption of Li during later cycles, the capacity fade will be more severe in a Li-ion cell than in a half-cell. It is thus important to measure the capacity retention and columbic efficiency of alloy anodes in a full Li-ion cell for long-term cyclability [188].

4.3. Rate and temperature dependence

A limited number of studies has been performed on the rate capacity of alloy anodes; several are shown in Fig. 8 [47,62,83,93,108,155,166]. The Sb/Al_2O_3/C nanocomposite had excellent rate capacity up to 5C [47]. Here, 5C was defined as the full use of the charge capacity (500 mAh g^{-1}) in 1/5 (0.2) h. The SnSb/C [62] and Sb/C [83] nanocomposites also showed a relatively stable rate capacity to the maximum rate tested (2C). The good rate capacity of the Sb/Al_2O_3/C and Sb/C nanocomposites was attributed to (a) the short lithium-diffusion distance and the high diffusion rate in the nanosized Sb particles and (b) the good electronic conductivity provided by the carbon matrix [47,83]. However, the specific capacities of microsized $NiSb_2$ powders decreased linearly as the C rate increased [166]. It is unclear whether the poor rate capacity of this sample was due to its large particle size. Capacity reduction at high C rates was also observed in Si-thin-film and Si-nanowire anodes [93,108]. More research is merited to understand the rate capacity of alloy anodes.

Temperature tolerance is an important requirement in many applications for lithium-ion batteries. The influence of temperature on the electrochemical performance of alloy anodes has not yet been well investigated. It has been observed that increasing the testing temperature from 30 to 50 °C almost doubled the capacity of an amorphous SiSn thin-film anode at high charge rate but had little effect at low charge rate [119]. A Sb/Al_2O_3/C nanocomposite exhibited a higher reversible capacity at 55 °C than at 25 °C (596 vs. 463 mAh g^{-1}) [47] but its capacity retention after 100 cycles decreased from 93% to 83% when the temperature was increased. The temperature effect is especially important for nanosized alloy anodes because of their small particle size and high surface area. At high temperature, the improved lithium diffusion and reaction kinetics may increase the capacity delivery and rate capacity of alloy anodes. However, the cyclic and calendar life of anode with fine particle sizes can be severely challenged due to the increased tendencies for microstructural instability, particle aggregation, anode/electrolyte reaction and catalytic effects on SEI formation. Therefore, the temperature tolerance (−30 to 50 °C) of alloy anodes deserves special attention in future studies.

5. Engineering design of alloy anodes

Large volume change is one of the major concerns for alloy anode design and development. However, large volume change in anode materials has been managed fairly well in commercial battery systems such as in nickel/cadmium and lead/acid batteries [5]. The Ni/Cd battery is based on a Cd/$Cd(OH)_2$ anodic reaction with a volume expansion of 130%. The traditional lead/acid battery cycled through PbO_2/$PbSO_4$ and Pb/$PbSO_4$ reaction with up to 120% volume change [5]. The many alloy materials discussed above demonstrate that long cycle life of several hundreds of cycles can be achieved by designing nanocomposite structures.

In practical cell design it is always highly desirable to maximize the electrochemical performance of a battery cell at a given size and limited volume change. Obrovac et al. [169] recently stressed that the volumetric energy density of the active material is more important than the specific energy density because of the restricted size requirements of battery cells for many consumer applications and because of the high cost of the extra supporting materials required such as binder, conductive carbon and foils, which are associated with low volumetric energy density. Interestingly, they calculated the volumetric energy density of different anode materials and

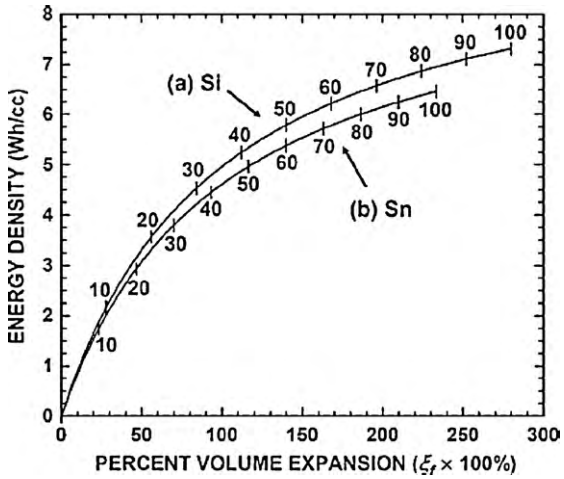

Fig. 9. Universal energy–expansion curves (vs. a 3.75-V cathode) for (a) silicon and (b) tin alloys with inactive components calculated from silicon and tin voltage curves during delithiation. Indicated on the curves is the volume percent of electrochemically active silicon or tin in the alloy. Reproduced from [169] with permission.

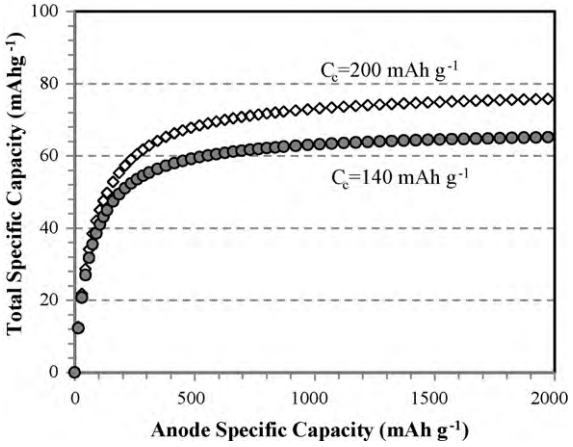

Fig. 10. Total capacity of an 18,650 Li-ion cell as a function of anode capacity, including masses of other required internal components and case. Capacities of the cathodes (Cc) considered were 140 and 200 mAh g^{-1} [9].

found that many active elements have nearly same (volumetric) energy density at a given volume expansion because the molar volume of lithium is nearly the same in any lithium alloy and independent of the lithium content [169]. It was also shown that alloying inactive elements with active elements actually increased the volumetric energy density, which is another strong supporting argument for using inactive-matrix nanocomposite structures.

Fig. 9 shows an example of the universal energy–expansion curves calculated for silicon and tin alloys [169]. The energy densities of Si and Sn alloys at a given volume expansion are fairly close and the slightly lower energy density of tin than silicon alloy is due to its higher average voltage for the delithiation half-cycle (0.65 V for Sn vs. 0.42 V for Si). Obrovac et al. suggested that these universal energy–expansion curves are a powerful tool for the design of anode materials [169]. For example, for an electrode system that can withstand a maximum of 100% volume expansion the curve shows that the highest energy density can be achieved for Si-based alloy is 5 Wh cm^{-3} with a composition of 36 vol.% active silicon and 64 vol.% inactive phases.

A second consideration for anode design is whether or not it is necessary to pursue the maximum specific capacity of alloy materials. In a recent paper, Kasavajjula et al. [9] calculated the specific capacity of a Li-ion cell as a function of the capacity of anode material (see Fig. 10). They concluded that the total cell capacity increased noticeably when increasing the anode capacity up to 1000–1200 mAh g^{-1} (the cathode capacity considered was 140–200 mAh g^{-1}). Above this level, the improvement in total cell capacity was marginal. This conclusion supports the use of approaches such as multiphase composites and cycling-voltage control in practical cell design for Si-based alloys. A recent study indicated that it is feasible to operate practical battery cells in a controlled-voltage profile [133].

6. Conclusions

Thanks to extensive research efforts, the electrochemical performance of alloy anodes has been significantly improved in recent years. Advanced alloy anodes have been developed with a long cycle life of over 300 cycles and a reversible capacity of 500–700 mAh g^{-1}. The capacity fade rates of these alloy materials are as low as 0.07% per cycle. Simultaneously, the first-cycle irreversible capacity loss of alloy anodes can be reduced to 50–100 mAh g^{-1}, corresponding to a high initial coulombic efficiency of ~90%. The cause of first-cycle capacity loss has been attributed to (a) a loss of active material, (b) SEI formation, (c) Li trapping in the host alloy, (d) reaction with oxide impurities and (e) the aggregation of active particles. The key to reducing the irreversible capacity of alloy anodes is to improve the purity of the alloy material, increase the primary particle size and reduce the capacity loss incurred by the (carbon) matrix.

The approaches used for improving cycling performance of alloy anodes include (a) multiphase composites, (b) porous anode structures, (c) reducing active particle size, (d) intermetallic phases, (e) thin-film and amorphous alloys, (f) cycling-voltage control and (g) binder and electrolyte modification. Among these, the multiphase carbon-matrix nanocomposites showed the most promising performance for practical use. The selection of binder and electrolyte has significant impacts on the cycle life of alloy anodes. Further research is needed to address the practical requirements for alloy anodes including high-rate performance, temperature dependence, abuse tolerance and long-term stability.

Acknowledgements

The author would like to thank Prof. Gary Tepper and Dr. Russell Jamison for a visiting professorship at Virginia Commonwealth University.

References

[1] B. Scosati, J. Garche, J. Power Sources 195 (2010) 2419.
[2] A.S. Arico, P. Bruce, B. Scrosati, J.M. Tarascon, W.V. Schalkwijk, Nature 4 (2005) 366.
[3] A.K. Shukla, T.P. Kumar, Curr. Sci. 94 (2008) 314.
[4] M. Winter, J.O. Besenhard, M.E. Spahr, P. Novak, Adv. Mater. 10 (1998) 725.
[5] D. Larcher, S. Beattie, M. Morcrette, K. Edstrom, J.C. Jumas, J.M. Tarascon, J. Mater. Chem. 17 (2007) 3759.
[6] M.M. Thackeray, J.T. Vaughey, L.M.L. Fransson, J. Met. 54 (2002) 20.
[7] M. Winter, J.O. Besenhard, Electrochim. Acta 45 (1999) 31.
[8] R. Benedek, M.M. Thackeray, J. Power Sources 110 (2002) 406.
[9] U. Kasavajjula, C. Wang, A.J. Appleby, J. Power Sources 163 (2007) 1003.
[10] W.J. Weydanz, M. Wohlfahrt-Mehrens, R.A. Huggins, J. Power Sources 81–82 (1999) 237.
[11] H. Kim, J. Choi, H.J. Sohn, T. Kang, J. Electrochem. Soc. 146 (1999) 4401.
[12] B. Gao, S. Sinha, L. Fleming, O. Zhou, Adv. Mater. 13 (2001) 816.
[13] J. Yang, M. Wachtler, M. Winter, J.O. Besenhard, Electrochem. Solid-State Lett. 2 (1999) 161.
[14] J. Yang, Y. Takeda, N. Imanishi, O. Yamamoto, J. Electrochem. Soc. 146 (1999) 4009.
[15] H. Li, L. Shi, W. Lu, X. Huang, L. Chen, J. Electrochem. Soc. 148 (2001) A915.
[16] M. Wachtler, M. Winter, J.O. Besenhard, J. Power Sources 105 (2002) 151.
[17] M. Wachtler, J.O. Besenhard, M. Winter, J. Power Sources 94 (2001) 189.
[18] J.W. Kim, J.H. Ryu, K.T. Lee, S.M. Oh, J. Power Sources 147 (2005) 227.
[19] C. Wang, A.J. Appleby, F.E. Little, J. Power Sources 93 (2001) 174.
[20] J.T. Vaughey, L. Fransson, H.A. Swinger, K. Edstrom, M.M. Thackeray, J. Power Sources 119–121 (2003) 64.

[21] L.Y. Beaulieu, K.W. Eberman, R.L. Turner, L.J. Krause, J.R. Dahn, Electrochem. Solid-State Lett. 4 (2001) A137.
[22] A. Ulus, Y. Rosenberg, L. Burstein, E. Peled, J. Electrochem. Soc. 149 (2002) A635.
[23] J.H. Ryu, J.W. Kim, Y.E. Sung, S.M. Oh, Electrochem. Solid-State Lett. 7 (2004) A306.
[24] H. Li, X. Huang, L. Chen, Electrochem. Solid-State Lett. 1 (1998) 241.
[25] R. Alcantara, F.J. Fernandez-Madrigal, P. Lavela, J.L. Tirado, J.C. Jumas, J. Olivier-Fourcade, J. Mater. Chem. 9 (1999) 2517.
[26] M. Stjerndahl, H. Bryngelsson, T. Gustafsson, J.T. Vaughey, M.M. Thackeray, K. Edstrom, Electrochim. Acta 52 (2007) 4947.
[27] M.R. Wagner, P.R. Raimann, A. Trifonova, K.C. Moeller, J.O. Besenhard, M. Winter, Electrochem. Solid-State Lett. 7 (2004) A201.
[28] L.Y. Beaulieu, S.D. Beattie, T.D. Hatchard, J.R. Dahn, J. Electrochem. Soc. 150 (2003) A419.
[29] J.M. Tarascon, M. Morcrette, L. Dupont, Y. Chabre, C. Payen, D. Larcher, V. Pralong, J. Electrochem. Soc. 150 (2003) A732.
[30] P. Limthongkul, Y.I. Jang, N.J. Dudney, Y.M. Chiang, J. Power Sources 119–121 (2003) 604.
[31] P.P. Ferguson, R.A. Dunlap, J.R. Dahn, J. Electrochem. Soc. 157 (2010) A326.
[32] Z. Huang, S. Hu, X. Hou, Q. Ru, H. Yu, L. Zhao, W. Li, Chin. Sci. Bull. 54 (2009) 1003.
[33] H. Li, L. Shi, Q. Wang, L. Chen, X. Huang, Solid State Ionics 148 (2002) 247.
[34] S. Matsuno, M. Noji, T. Kashiwagi, M. Nakayama, M. Wakihara, J. Phys. Chem. C 111 (2007) 7548.
[35] H. Lia, X. Huang, L. Chen, G. Zhou, Z. Zhang, D. Yu, Y.J. Mo, N. Pei, Solid State Ionics 135 (2000) 181.
[36] G.W. Zhou, H. Li, H.P. Sun, D.P. Yu, Y.Q. Wang, X.J. Huang, L.Q. Chen, Z. Zhang, Appl. Phys. Lett. 75 (1999) 2447.
[37] C. Park, Y.U. Kim, H. Kim, H.J. Sohn, J. Power Sources 158 (2006) 1451.
[38] G.A. Roberts, E.J. Cairns, J.A. Reimer, Electrochem. J. Soc. 151 (2004) A493.
[39] A. Trifonova, M. Wachtler, M.R. Wagner, H. Schroettner, C. Mitterbauer, F. Hofer, K.C. Moller, M. Winter, J.O. Besenhard, Solid State Ionics 168 (2004) 51.
[40] Y. Idot, T. Kubota, A. Matsufuji, Y. Maekawa, T. Miyasaka, Science 276 (1997) 1395.
[41] I.A. Courtney, W.R. McKinnon, J.R. Dahn, J. Electrochem. Soc. 146 (1999) 59.
[42] J. Yang, M. Winter, J.O. Besenhard, Solid State Ionics 90 (1996) 281.
[43] O. Mao, R.L. Turner, I.A. Courtney, B.D. Fredericksen, M.I. Buckett, L.J. Krause, J.R. Dahn, Electrochem. Solid-State Lett. 2 (1999) 3.
[44] K.D. Kepler, J.T. Vaughey, M.M. Thackeray, J. Power Sources 81–82 (1999) 383.
[45] M.A. Reddy, U.V. Varadaraju, J. Power Sources 159 (2006) 336.
[46] T. Li, Y.L. Cao, X.P. Ai, H.X. Yang, J. Power Sources 184 (2008) 473.
[47] S. Yoon, A. Manthiram, Chem. Mater. 21 (2009) 3898.
[48] H.Y. Lee, S.M. Lee, Electrochem. Commun. 6 (2004) 465.
[49] Y. Liu, Z.Y. Wen, X.Y. Wang, X.L. Yang, A. Hiranoc, N. Imanishic, Y. Takeda, J. Power Sources 189 (2009) 480.
[50] I. Kim, P.N. Kumta, G.E. Blomgren, Electrochem. Solid-State Lett. 3 (2000) 493.
[51] G.J. Jeong, Y.U. Kim, H.J. Sohn, T. Kang, J. Power Sources 101 (2001) 201.
[52] I. Kim, G.E. Blomgren, P.N. Kumta, Electrochem. Solid-State Lett. 6 (2003) A157.
[53] I.A. Courtney, J.R. Dahn, J. Electrochem. Soc. 144 (1997) 2045.
[54] M.D. Fleischauer, M.N. Obrovac, J.D. McGraw, R.A. Dunlap, J.M. Topple, J.R. Dahn, J. Electrochem. Soc. 153 (2006) A484.
[55] J.T. Vaughey, J. Owejan, M.M. Thackeray, Electrochem. Solid-State Lett. 10 (2007) A220.
[56] J. Wolfenstine, J. Power Sources 124 (2003) 241.
[57] J. Saint, M. Morcrette, D. Larcher, L. Laffont, S. Beattie, J.P. Peres, D. Talaga, M. Couzi, J.M. Tarascon, Adv. Funct. Mater. 17 (2007) 1765.
[58] F. Wang, M. Zhao, X. Song, J. Power Sources 175 (2008) 558.
[59] F.J. Fernandez-Madrigal, P. Lavela, C.P. Vicente, J.L. Tirado, J.C. Jumas, J. Olivier-Fourcade, Chem. Mater. 14 (2002) 2962.
[60] H. Mukaibo, T. Osaka, P. Reale, S. Panero, B. Scrosati, M. Wachtler, J. Power Sources 132 (2004) 225.
[61] J. Yang, Y. Takeda, N. Imanishi, J.Y. Xie, O. Yamamoto, Solid State Ionics 133 (2000) 189.
[62] C.M. Park, H.J. Sohn, Electrochim. Acta 54 (2009) 6367.
[63] J.T. Vaughey, C.S. Johnson, A.J. Kropf, R. Benedek, M.M. Thackery, H. Tostmann, T. Sarakonsri, S. Hackney, L. Fransson, K. Edstrom, J.O. Thomas, J. Power Sources 97–98 (2001) 194.
[64] J.T. Vaughey, J. O'Hara, M.M. Thackeray, Electrochem. Solid-State Lett. 3 (2000) 13.
[65] K.C. Hewitt, L.Y. Beaulieu, J.R. Dahn, J. Electrochem. Soc. 148 (2001) A402.
[66] T. Sarakonsri, C.S. Johnson, S.A. Hackney, M.M. Thackeray, J. Power Sources 153 (2006) 319.
[67] H. Tostmann, A.J. Kropf, C.S. Johnson, J.T. Vaughey, M.M. Thackeray, Phys. Rev. B 66 (2002) 14106.
[68] C.S. Johnson, J.T. Vaughey, M.M. Thackeray, T. Sarakonsri, S.A. Hackney, L. Fransson, K. Edstrom, J.O. Thomas, Electrochem. Commun. 2 (2000) 595.
[69] X. Wang, Z. Wen, B. Lin, J. Lin, X. Wu, X. Xu, J. Power Sources 184 (2008) 508.
[70] J. Yin, M. Wada, S. Yoshida, K. Ishihara, S. Tanase, T. Sakaia, J. Electrochem. Soc. 150 (2003) A1129.
[71] E. Ronnebro, J. Yin, A. Kitano, M. Wada, S. Tanase, T. Sakai, J. Electrochem. Soc. 151 (2004) A1738.
[72] M.L. Sui, K. Lu, W. Deng, L.Y. Xiong, S. Patu, Y.Z. He, Phys. Rev. B 44 (1991) 6466.
[73] J.R. Dahn, I.A. Courtney, O. Mao, Solid State Ionics 111 (1998) 289.
[74] H. Lee, Y. Kim, M. Hong, S. Lee, J. Power Sources 141 (2005) 159.
[75] Q. Si, K. Hanai, N. Imanishi, M. Kubo, A. Hirano, Y. Takeda, O. Yamamoto, J. Power Sources 189 (2009) 761.
[76] Z. Luo, D. Fan, X. Liu, H. Mao, C. Yao, Z. Deng, J. Power Sources 189 (2009) 16.
[77] C.M. Park, H.J. Sohn, J. Electrochem. Soc. 157 (2010) A46.
[78] M. Yoshio, H. Wang, K. Fukuda, T. Umeno, N. Dimov, Z. Ogumib, J. Electrochem. Soc. 149 (2002) A1598.
[79] W. Liu, Z. Guo, W. Young, D. Shieh, H. Wu, M. Yang, N. Wu, J. Power Sources 140 (2005) 139.
[80] H. Li, X. Huang, L. Chen, Z. Wu, Y. Liang, Electrochem. Solid-State Lett. 2 (1999) 547.
[81] C.S. Wang, G.T. Wu, X.B. Zhang, Z.F. Qi, W.Z. Li, J. Electrochem. Soc. 145 (1998) 2751.
[82] Y. Liu, K. Hanai, K. Horikawa, N. Imanishi, A. Hirano, Y. Takeda, Mater. Chem. Phys. 89 (2005) 80.
[83] C.M. Park, S. Yoon, S.I. Lee, J.H. Kim, J.H. Jung, H.J. Sohn, J. Electrochem. Soc. 154 (2007) A917.
[84] N. Ding, J. Xu, Y. Yao, G. Wegner, I. Lieberwirth, C. Chen, J. Power Sources 192 (2009) 644.
[85] L. Trahey, J.T. Vaughey, H.H. Kung, M.M. Thackeray, J. Electrochem. Soc. 156 (2009) A385.
[86] M. Yoshio, T. Tsumura, N. Dimov, J. Power Sources 146 (2005) 10.
[87] L. Huang, Y. Yang, L. Xue, H. Wei, F. Ke, J. Li, S. Sun, Electrochem. Commun. 11 (2009) 6.
[88] H. Zhao, C. Jiang, X. He, J. Ren, J. Power Sources 184 (2008) 532.
[89] K. Nishikawa, K. Dokko, K. Kinoshita, S.W. Woo, K. Kanamura, J. Power Sources 189 (2009) 726.
[90] L. Huang, H. Wei, Fu. Ke, X. Fan, J. Li, S. Sun, Electrochim. Acta 54 (2009) 2693.
[91] X. Fan, Q. Zhuang, G. Wei, L. Huang, Q. Dong, S. Sun, J. Appl. Electrochem. 39 (2009) 1323.
[92] I.A. Courtney, J.R. Dahn, J. Electrochem. Soc. 144 (1997) 2943.
[93] C.K. Chan, H. Peng, G. Liu, K. Mcilwrath, X.F. Zhang, R.A. Huggins, Y. Cui, Nat. Nanotechnol. 3 (2008) 31.
[94] H. Li, Z. Wang, L. Chen, X. Huang, Adv. Mater. 21 (2009) 4593.
[95] L.Y. Beaulieu, D. Larcher, R.A. Dunlap, J.R. Dahn, J. Electrochem. Soc. 147 (2000) 3206.
[96] A.D.W. Todd, P.P. Ferguson, J.G. Barker, M.D. Fleischauer, J.R. Dahn, J. Electrochem. Soc. 156 (2009) A1034.
[97] L. Fransson, E. Nordstrom, K. Edstrom, L. Haggstrom, J.T. Vaughey, M.M. Thackeray, J. Electrochem. Soc. 149 (2002) A736.
[98] M. Morcrette, D. Larcher, J.M. Tarascon, K. Edstrom, J.T. Vaughey, M.M. Thackeray, Electrochim. Acta 52 (2007) 5339.
[99] L.M.L. Fransson, J.T. Vaughey, R. Benedek, K. Edstrom, J.O. Thomas, M.M. Thackeray, Electrochem. Commun. 3 (2001) 317.
[100] D.G. Kim, H. Kim, H.J. Sohn, T. Kang, J. Power Sources 104 (2002) 221.
[101] J. Wolfenstine, S. Campos, D. Foster, J. Read, W.K. Behl, J. Power Sources 109 (2002) 230.
[102] S. Matsuno, M. Noji, M. Nakayama, M. Wakihara, Y. Kobayashi, H. Miyashirob, J. Electrochem. Soc. 155 (2008) A151.
[103] M. Nakayama, S. Matsuno, J. Shirakawa, M. Wakihara, J. Electrochem. Soc. 155 (2008) A505.
[104] S. Matsuno, M. Nakayama, M. Wakihara, J. Electrochem. Soc. 155 (2008) A61.
[105] S. Ohara, J. Suzuki, K. Sekine, T. Takamura, J. Power Sources 136 (2004) 303.
[106] J.P. Maranchi, A.F. Hepp, P.N. Kumta, Electrochem. Solid-State Lett. 6 (2003) A198.
[107] J.B. Kim, H.Y. Lee, K.S. Lee, S.H. Lim, S.M. Lee, Electrochem. Commun. 5 (2003) 544.
[108] T. Takamura, S. Ohara, M. Uehara, J. Suzuki, K. Sekine, J. Power Sources 129 (2004) 96.
[109] J. Graetz, C.C. Ahn, R. Yazami, B. Fultz, Electrochem. Solid-State Lett. 6 (2003) A194.
[110] S. Ohara, J. Suzuki, K. Sekine, T. Takamura, J. Power Sources 119–121 (2003) 591.
[111] K.L. Lee, J.Y. Jung, S.W. Lee, H.S. Moon, J.W. Park, J. Power Sources 129 (2004) 270.
[112] L.B. Chen, J.Y. Xie, H.C. Yu, T.H. Wang, J. Appl. Electrochem. 39 (2009) 1157.
[113] T.D. Hatchard, M.N. Obrovac, J.R. Dahn, J. Electrochem. Soc. 153 (2006) A282.
[114] T. Moon, C. Kim, B. Park, J. Power Sources 155 (2006) 391.
[115] T. Takamura, M. Uehara, J. Suzuki, K. Sekine, K. Tamura, J. Power Sources 158 (2006) 1401.
[116] T. Zheng, J.S. Xue, J.R. Dahn, Chem. Mater. 8 (1996) 389.
[117] S.W. Song, K.A. Striebel, R.P. Reade, G.A. Roberts, E.J. Cairnsa, J. Electrochem. Soc. 150 (2003) A121.
[118] Z. Chen, V. Chevrier, L. Christensen, J.R. Dahn, Electrochem. Solid-State Lett. 7 (2004) A310.
[119] L.Y. Beaulieu, K.C. Hewitt, R.L. Turner, A. Bonakdarpour, A.A. Abdo, L. Christensen, K.W. Eberman, L.J. Krause, J.R. Dahn, J. Electrochem. Soc. 150 (2003) A149.
[120] T.D. Hatchard, J.R. Dahn, S.T. Russler, M. Fleischauer, A. Bonakdarpour, J.R. Mueller-Neuhaus, K.C. Hewitt, Thin Solid Films 443 (2003) 144.
[121] M.D. Fleischauer, M.N. Obrovac, J.R. Dahn, J. Electrochem. Soc. 153 (2006) A1201.
[122] T.D. Hatchard, M.N. Obrovac, J.R. Dahn, J. Electrochem. Soc. 152 (2005) A2335.
[123] M.D. Fleischauer, J.M. Topple, J.R. Dahn, Electrochem. Solid-State Lett. 8 (2005) A137.
[124] Y.L. Kim, S.J. Lee, H.K. Baik, S.M. Lee, J. Power Sources 119–121 (2003) 106.

[125] K.S. Lee, Y.L. Kim, S.M. Lee, J. Power Sources 146 (2005) 464.
[126] H. Mukaibo, T. Momma, T. Osaka, J. Power Sources 146 (2005) 457.
[127] M.D. Fleischauer, J.R. Dahn, J. Electrochem. Soc. 151 (2004) A1216.
[128] O. Mao, J.R. Dahn, J. Electrochem. Soc. 146 (1999) 414.
[129] H. Kim, Y.J. Kim, D.G. Kim, H.J. Sohn, T. Kang, Solid State Ionics 144 (2001) 41.
[130] Y.U. Kim, C.K. Lee, H.J. Sohn, T. Kang, J. Electrochem. Soc. 151 (2004) A933.
[131] H. Jung, M. Park, Y.G. Yoon, G.B. Kim, S.K. Joo, J. Power Sources 115 (2003) 346.
[132] M.N. Obrovac, L. Christensen, Electrochem. Solid-State Lett. 7 (2004) A93.
[133] M.N. Obrovac, L.J. Krause, J. Electrochem. Soc. 154 (2007) A103.
[134] O. Crosnier, X. Devaux, T. Brousse, P. Fragnaud, D.M. Schleich, J. Power Sources 97–98 (2001) 188.
[135] W.R. Liu, M.H. Yang, H.C. Wu, S.M. Chiao, N.L. Wu, Electrochem. Solid-State Lett. 8 (2005) A100.
[136] Z. Chen, L. Christensen, J.R. Dahn, Electrochem. Commun. 5 (2003) 919.
[137] J. Li, R.B. Lewis, J.R. Dahn, Electrochem. Solid-State Lett. 10 (2007) A17.
[138] G.X. Wang, J. Yao, H.K. Liu, Electrochem. Solid-State Lett. 7 (2004) A250.
[139] Z.P. Guo, J.Z. Wang, H.K. Liu, S.X. Dou, J. Power Sources 146 (2005) 448.
[140] Q. Si, K. Hanai, T. Ichikawa, A. Hirano, N. Imanishi, Y. Takeda, O. Yamamoto, J. Power Sources 195 (2010) 1720.
[141] I.S. Kim, P.N. Kumta, J. Power Sources 136 (2004) 145.
[142] M. Holzapfel, H. Buqa, W. Scheifele, P. Novak, F.M. Petrat, Chem. Commun. 12 (2005) 1566.
[143] M. Holzapfel, H. Buqa, F. Krumeich, P. Novak, F.M. Petrat, C. Veit, Electrochem. Solid-State Lett. 8 (2005) A516.
[144] Z.S. Wen, J. Yang, B.F. Wang, K. Wang, Y. Liu, Electrochem. Commun. 5 (2003) 165.
[145] H. Kim, D. Im, S.G. Doo, J. Power Sources 174 (2007) 588.
[146] T.D. Hatchard, J.R. Dahn, J. Electrochem. Soc. 151 (2004) A838.
[147] F. Disma, L. Aymard, L. Dupont, J.M. Tarascon, J. Electrochem. Soc. 143 (1996) 3959.
[148] T. Morita, N. Takami, J. Electrochem. Soc. 153 (2006) A245.
[149] G.X. Wang, J.H. Ahn, J. Yao, S. Bewlay, H.K. Liu, Electrochem. Commun. 6 (2004) 689.
[150] C.H. Doh, H.M. Shin, D.H. Kim, Y.D. Chuang, S.I. Moon, B.S. Jin, H.S. Kim, K.W. Kim, D.H. Oh, A. Veluchamy, Bull. Korean Chem. Soc. 29 (2008) 309.
[151] J.H. Park, D.H. Joeng, S.M. Cha, Y.K. Sun, C.S. Yoon, J. Power Sources 188 (2009) 281.
[152] H.Y. Lee, S.M. Lee, J. Power Sources 112 (2002) 649.
[153] J.M. Yan, H.Z. Huang, J. Zhang, Y. Yang, J. Power Sources 175 (2008) 547.
[154] K.M. Lee, Y.S. Lee, Y.W. Kim, Y.K. Sun, S.M. Lee, J. Alloys Compd. 472 (2009) 461.
[155] J. Hassoun, S. Panero, G. Mulas, B. Scrosati, J. Power Sources 171 (2007) 928.
[156] G. Wang, Z.W. Lu, X.P. Gao, X.J. Liu, J.Q. Wang, J. Power Sources 189 (2009) 655.
[157] H. Sakaguchi, H. Honda, Y. Akasaka, T. Esaka, J. Power Sources 119–121 (2003) 50.
[158] H. Guo, H. Zhao, X. Jia, Electrochem. Commun. 9 (2007) 2207.
[159] J.J. Zhang, Y.M. Zhang, X. Zhang, Y.Y. Xia, J. Power Sources 167 (2007) 171.
[160] X.B. Zhao, G.S. Cao, Electrochim. Acta 46 (2001) 891.
[161] F.J. Fernandez-Madrigal, P. Lavela, C. Perez-Vicente, J.L. Tirado, J. Electroanal. Chem. 501 (2001) 205.
[162] J. Xie, X.B. Zhao, G.S. Cao, M.J. Zhao, S.F. Su, J. Alloys Compd. 393 (2005) 283.
[163] X.B. Zhao, Y.D. Zhong, G.S. Cao, J. Zhejiang Univ. Sci. 5 (2004) 418.
[164] C. Villevieille, B. Fraisse, M. Womes, J.C. Jumas, L. Monoconduit, J. Power Sources 189 (2009) 324.
[165] H. Honda, H. Sakaguchi, I. Tanaka, T. Esaka, J. Power Sources 123 (2003) 216.
[166] C. Villevieille, C.M. Ionic-Bousquet, B. Ducorant, J.C. Jumas, L. Monoconduit, J. Power Sources 172 (2007) 388.
[167] P.P. Ferguson, P. Liao, R.A. Dunlap, J.R. Dahn, J. Electrochem. Soc. 156 (2009) A13.
[168] H. Jung, M. Park, Y.G. Yoon, G.B. Kim, S.K. Joo, J. Power Sources 115 (2003) 246.
[169] M.N. Obrovac, L. Christensen, D.B. Le, J.R. Dahn, J. Electrochem. Soc. 154 (2007) A849.
[170] O. Mao, R.A. Dunlap, J.R. Dahn, J. Electrochem. Soc. 146 (1999) 405.
[171] B.A. Boukamp, G.C. Lesh, R.A. Huggins, J. Electrochem. Soc. 128 (1981) 725.
[172] J.O. Besenhard, J. Yang, M. Winter, J. Power Sources 68 (1997) 87.
[173] M.M. Thackeray, J.T. Vaughey, C.S. Johnson, A.J. Kropf, R. Benedek, L.M.L. Fransson, K. Edstrom, J. Power Sources 113 (2003) 124.
[174] T.J. Richardson, G. Chen, J. Power Sources 174 (2007) 810.
[175] S.D. Beattie, J.R. Dahn, J. Electrochem. Soc. 152 (2005) C542.
[176] J.R. Dahn, I.A. Courtney, O. Mao, Solid State Ionics 111 (1998) 289.
[177] X. Wang, Z. Wen, Y. Liu, X. Xu, J. Lin, J. Power Sources 189 (2009) 121.
[178] J.H. Kim, H. Kim, H.J. Sohn, Electrochem. Commun. 7 (2005) 557.
[179] B. Lestriez, S. Bahri, I. Sandu, L. Roue, D. Guyomard, Electrochem. Commun. 9 (2007) 2801.
[180] N.S. Hochgatterer, M.R. Schweiger, S. Koller, P.R. Raimann, T. Wohrle, C. Wurm, M. Winter, Electrochem. Solid-State Lett. 11 (2008) A76.
[181] L. Chen, X. Xie, J. Xie, K. Wang, J. Yang, J. Appl. Electrochem. 36 (2006) 1099.
[182] N.S. Choi, K.H. Yew, W.U. Choi, S.S. Kim, J. Power Sources 177 (2008) 590.
[183] J. Li, D.B. Le, P.P. Ferguson, J.R. Dahn, Electrochim. Acta 55 (2010) 2991.
[184] M.Q. Li, M.Z. Qu, X.Y. He, Z.L. Yu, Electrochim. Acta 54 (2009) 4506.
[185] I.A. Profatilova, N.S. Choi, K.H. Yew, W.U. Choi, Solid State Ionics 179 (2008) 2399.
[186] N.S. Choi, K.H. Yew, K.Y. Lee, M. Sung, H. Kim, S.S. Kim, J. Power Sources 161 (2006) 1254.
[187] G.B. Han, M.H. Ryou, K.Y. Cho, Y.M. Lee, J.K. Park, J. Power Sources 195 (2010) 3709.
[188] A.J. Smith, J.C. Burns, S. Trussler, J.R. Dahn, J. Electrochem. Soc. 157 (2010) A196.
[189] C.C. Nguyen, S.W. Song, Electrochim. Acta 55 (2010) 3026.
[190] J. Zhao, L. Wang, X. He, C. Wan, C. Jiang, Electrochim. Acta 53 (2008) 7048.
[191] J. Hassoun, A. Fernicola, M.A. Navarra, S. Panero, B. Scrosati, J. Power Sources 195 (2010) 574.
[192] H. Zhao, Z. Zhu, C. Yin, H. Guo, D.H.L. Ng, Mater. Chem. Phys. 110 (2008) 201.
[193] L.B. Chen, J.Y. Xie, H.C. Yu, T.H. Wang, Electrochim. Acta 53 (2008) 8149.
[194] P. Gu, R. Cai, Y. Zhou, Z. Shao, Electrochim. Acta 55 (2010) 3876.
[195] N. Ding, J. Xu, Y. Yao, G. Wegner, I. Lieberwith, C. Chen, J. Power Sources 192 (2009) 644.
[196] J.M. Lee, H. Jung, Y. Hwa, H. Kim, D. Im, S.G. Doo, H.J. Sohn, J. Power Sources 195 (2010) 5044.
[197] Z.Y. Zeng, J.P. Tu, Y.Z. Yang, J.Y. Xiang, X.H. Huang, F. Mao, M. Ma, Electrochim. Acta 53 (2008) 2724.
[198] S. Liu, Q. Li, Y. Chen, F. Zhang, J. Alloys Compd. 478 (2009) 694.
[199] H.H. Chang, H.C. Wu, N.L. Wu, Electrochem. Commun. 10 (2008) 1823 (#189).
[200] H.H. Chang, C.C. Chang, C.Y. Su, H.C. Wu, M.H. Yang, N.L. Wu, J. Power Sources 185 (2008) 466.
[201] J. Schiotz, K.W. Jacobsen, Science 301 (2003) 1537.
[202] L. Lu, X. Chen, X. Huang, K. Lu, Science 323 (2009) 607.
[203] X. Zhu, R. Birringer, U. Herr, H. Gleiter, Phys. Rev. B 35 (1987) 9085.